

optically generated LO signal from the second DIP output. In a complete radio-over-fibre system this 140MHz signal would be transmitted via a conventional fibre optic link back to the CS.

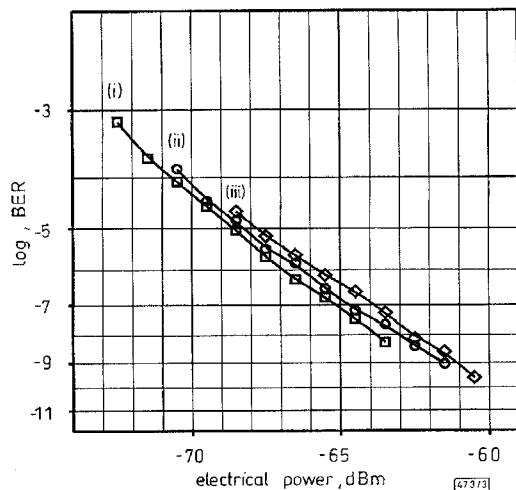


Fig. 3 BER against electrical power at OQPSK receiver input

Modulation: 140Mbit/s, CMI-coded, PRBS, word length $2^{23}-1$
 (i) back-to-back measurement; bidirectional transmission via microwave links between BS and MS
 (ii) fibre length between CS and BS: 10m (standard singlemode fibre)
 (iii) fibre length between CS + BS: 12.8km (standard singlemode fibre)

To investigate the optical microwave transmission and generation, bit error rate (BER) measurements (Fig. 3) were carried out without a radio link. Fig. 3(i) gives the results of a back-to-back BER measurement at 140MHz when the OQPSK modulator and demodulator were connected directly by a coaxial cable. Fig. 3(ii) and (iii) give the BER values after transmission via the microwave links between MS and BS with different lengths of standard singlemode fibre between CS and BS. Fig. 3(ii) depicts BER values when using 10m SMF with an optical power of 1.4dBm at the OMC input, while Fig. 3(iii) shows BER values for 12.8km fibre length and -13.5dBm optical input power. To compare the different measurements the BER is given against electrical power which was varied using an attenuator in front of the OQPSK-demodulator. At a BER of 10^{-9} , only small penalties <1dB for the receiver sensitivity were measured and no error floor was observed. The measurements yielded an electrical dynamic range larger than 50dB in both cases.

Conclusion: 140Mbit/s-data signals in the OQPSK format were transmitted in a simplified experimental mobile communication system in the downstream and upstream directions with optically generated microwave carriers in the 18–20GHz band.

In this centralised concept, functions such as frequency generation, frequency selection, signal processing, and network management are performed in the control station. Hence, very simple, low cost base stations can be built, and even the control station requires only cheap, standard components for moderate microwave frequencies. Heterodyning the optical signals of two laser diodes offers great flexibility regarding the microwave frequency, since it is simply given by the frequency spacing of the two lasers. Additionally, the slave lasers are multifunctional in that they can be used to represent elements such as phase modulators whose required modulation rate is determined by the maximum system bitrate, as optical filters as well as amplifiers. In contrast to other optical microwave generation techniques, e.g. optical harmonic upconversion [10], the advantage of this technique is that the optical power is concentrated only in the two needed optical waves. Thus it represents a very efficient microwave generation technique which is also suitable for long distances without degradation due to fibre dispersion. Higher frequencies applying this technique are possible e.g. frequencies > 70GHz and phase noise cancellation by sideband injection locking up to 50GHz has been published [11].

Acknowledgment: The work was carried out within the national research programme Photonik II, supported by the Bundesministerium für Bildung, Wissenschaft, Forschung und Technologie and

by the city of Berlin. The authors would like to thank the Robert Bosch GmbH for providing the digital radio-relay system.

© IEE 1997

Electronics Letters Online No: 19970944

29 May 1997

R.-P. Braun, G. Grosskopf, D. Rohde and F. Schmidt (Heinrich-Hertz-Institut für Nachrichtentechnik Berlin GmbH, Einsteinufer 37, D-10587 Berlin, Germany)

R. Meschenmoser and G. Villino (Robert Bosch GmbH FV/SLH, PO Box 77 77 77, D-31132 Hildesheim, Germany)

References

- O'REILLY, J.J., LANE, P.M., CAPSTICK, M.H., SALGADO, H.M., HEIDEMANN, R., HOFSTETTER, R., and SCHMUCK, H.: 'RACE R2005: microwave optical duplex antenna link', *IEE Proc.*, 1993, **140**, (6), pp. 385–391
- HELMOLT, C.H.V., KRÜGER, U., KRÜGER, K., and KÜLLER, L.: '58GHz fibre optic upconverter applicable to wireless communication systems'. Optical Fibre Commun. Conf., OFC'96, San Jose, CA, USA, 1996, Paper ThC1
- KIM, D.Y., PELUSI, M., AHMED, Z., NOVAK, D., LIU, H.-F., and OGAWA, Y.: 'Ultrastable millimetre-wave signal generation using hybrid modelocking of a monolithic DBR laser', *Electron. Lett.*, 1995, **31**, (9), pp. 733–734
- SCHMUCK, H., and HEIDEMANN, R.: 'Hybrid fibre-radio field experiment at 60GHz'. 22th Europ. Conf. on Optical Commun., (ECOC'96), Oslo, Norway, September 1996, Vol. 4, Paper ThC.1.2, pp. 59–62
- WAKE, D., LIMA, C.R., and DAVIES, P.A.: 'Optical generation of millimeter-wave signals for fibre-radio systems using a dual-mode DFB semiconductor laser', *IEEE Trans.*, 1995, **MTT-43**, (9), pp. 2270–2276
- BRAUN, R.-P., KAISER, R., ROHDE, D., STENZEL, R., TROMMER, D., HEIDRICH, H., and GROSSKOPF, G.: 'Optical microwave generation and transmission experiments using a monolithically integrated tunable optical signal source'. 21st Europ. Conf. on Optical Commun., (ECOC'95), Brussels, Belgium, September 1995, Post-Deadline Paper
- GEORGES, J.B., PARK, J., SOLGAARD, O., PEPELJUGOSKI, P., SAYED, M., and LAU, K.Y.: 'Transmission of 300Mbit/s BPSK at 39GHz using feedforward optical modulation', *Electron. Lett.*, 1994, **30**, (2), pp. 160–161
- GOLDBERG, L., TAYLOR, H.F., WELLER, J.F., and BLOOM, D.M.: 'Microwave signal generation with injection-locked laser diodes', *Electron. Lett.*, 1983, **19**, (13), pp. 491–493
- KOBAYASHI, S., and KIMURA, T.: 'Optical phase modulation in an injection-locked AlGaAs semiconductor laser', *Electron. Lett.*, 1982, **18**, (5), pp. 210–211
- BRAUN, R.-P., GROSSKOPF, G., MESCHENMOSER, R., ROHDE, D., SCHMIDT, F., and VILLINO, G.: 'Optical harmonic upconversion for microwave generation in a bidirectional broadband mobile communication system', To be published
- BRAUN, R.-P., GROSSKOPF, G., ROHDE, D., and SCHMIDT, F.: 'Optical millimeter-wave generation and transmission experiments for mobile 60GHz-band communications', *Electron. Lett.*, 1996, **32**, (7), pp. 626–628

Modular mART for 3D target recognition

Eun-Soo Kim, Jin-Woo Cha and Chung-Sang Ryu

Indexing terms: Neural networks, Adaptive resonance theory

A modified adaptive resonance theory (mART) neural network of modular structure is proposed. The similarity function and weight resolution of the ART neural networks are modified, and the cluster merging algorithm and modular training method are both introduced. The results from 3D target recognition experiments are compared with those of a self-organising map (SOM) and single mART.

Introduction: Three dimensional object recognition is one of the most important issues in the military and industrial automation field. Accordingly, many reported methods to resolve this problem over recent decades have failed to give satisfactory results

[1]. This Letter is dedicated to providing a new approach using modular structure neural networks [2].

The algorithmic differences of the proposed modified adaptive resonance theory (mART) compared to the conventional ART [3] are the multi-bit weight resolution and the angular similarity test which correspond to the binary level and inner production in the conventional ART. The cluster combining step is added in the organisation procedure to suppress both the infinite creation of clusters and the generation of similar clusters [3]. Since each module is independent from the others, this structure can suppress class generalisation which generally occurs by excessive training.

mART and modular mART: The training and organising procedures of the proposed mART neural networks with modular structure are mainly composed of a clustering step, a merging step and a matching step. In the clustering step, the neural networks cluster the input feature maps according to the supervised learning concept within a specified class, and clusters similar to each other are combined in the merging step to prevent the database memory being wasted. Class limitation within the given teaching class in the clustering step is the key idea of the modular concept. This can be achieved by using additional registers specifying their own classes.

At the end of the self-organisation process, all the input patterns may be reentered into the matching networks for the class matching process. In this procedure, the weights of matching networks are mapped by the stochastic distribution information of maximum output scores obtained in the previous competitive organising networks. Also in this step, the interconnection is activated according to class. In the following, the learning algorithms are derived in respect of angular clustering of the input vectors.

Step 1: We initialise the weight matrix of $n \times M$ connected to the $C \times M$ output nodes of the upper layer as

$$\sum_{i=1}^n \sum_{j=1}^M w_{Cij} = \frac{1}{\sqrt{n}} \quad (1)$$

where C is the index of the classes. We also initialise the vigilance level ρ and the merging threshold σ with proper values between 0 and 1, and reset the count register T_{Cj} (where $j = 0, \dots, M$) to 0.

Step 2: Enter the unipolar input vector X_C to the input nodes after normalisation by

$$x'_{Ck} = \frac{x_{Ck}}{\sqrt{\sum_{i=1}^n (x_{Ci})^2}} \quad \text{for } k = 1, 2, \dots, N \quad (2)$$

and set for the specified class.

Step 3: Calculate all the matching scores y_{Cj} included in the class set according to

$$y_{Cj} = \sum_{i=1}^n w_{Cij} x_{Ci} \quad \text{for } j = 1, 2, \dots, M \quad (3)$$

In this step, the node m showing maximum score can be determined by

$$m = \operatorname{argmax}_{j=1,2,\dots,M} (y_{Cj}) \quad (4)$$

Step 4: Similarity test can be carried out by

$$\left| \frac{\angle_m}{\pi} - 1 \right| > \rho \quad (5)$$

The angular information \angle_m between the input vector and the winner neuron (i.e. m th neuron obtained by eqn. 4) can be calculated by

$$\angle_m = \cos^{-1} \left(\frac{\sum_{i=1}^n w_{Cim} x_{Ci}}{\|W_{Cm}\| \cdot \|X_C\|} \right) \quad (6)$$

where the $\|W_{Cm}\|$ and $\|X_C\|$ are defined as follows:

$$\|W_{Cm}\| \triangleq \sum_{i=1}^n |w_{Cim}| \quad (7)$$

$$\|X_C\| \triangleq \sum_{i=1}^n |x_{Ci}| \quad (8)$$

If the inequality in eqn. 5 is false, set variable m with the index of a free node to create a new cluster.

Step 5: Increase T_{Cm} , which indicates the number of patterns that show the best match with the dissolved cluster, and update the weights of the neuron selected in step 4 according to

$$w_{Cim}(t+1) = \frac{x_{Ci} + T_{Cm} \cdot w_{Cim}(t)}{T_{Cm} + 1} \quad (9)$$

This equation represents the update of either the newly appended or the existing winner cluster.

Step 6: Normalise the updated weight matrix using the normalisation method as in step 2.

Step 7: After the above clustering process, test the similarity between the dissolved cluster and the other clusters within the dissolved class using

$$\left| \frac{\angle_{m,n}}{\pi} - 1 \right| > \sigma \quad (10)$$

where

$$n = \operatorname{argmin}_{\substack{n=1,\dots,M \\ n \neq m}} \cos^{-1} \left(\frac{\sum_{i=1}^n w_{Cmi} w_{Cni}}{\|W_{Cm}\| \cdot \|W_{Cn}\|} \right) \quad (11)$$

If the inequality of eqn. 10 is false, go to step 2 for accepting the other input patterns.

Step 8: Merge the two clusters W_{Cm} and W_{Cn} by creating the weight W_{Cr} and the count register T_{Cr} as

$$W_{Cr} = \frac{W_{Cm} T_{Cm} + W_{Cn} T_{Cn}}{T_{Cm} + T_{Cn}} \quad (12)$$

and

$$T_{Cr} = T_{Cm} + T_{Cn} \quad (13)$$

Then reset the two dissolved clusters and go to step 6 to test again.

Step 9: Iterate the procedures from steps 2 to 8 until the output nodes of the upper layer reach certain steady states.

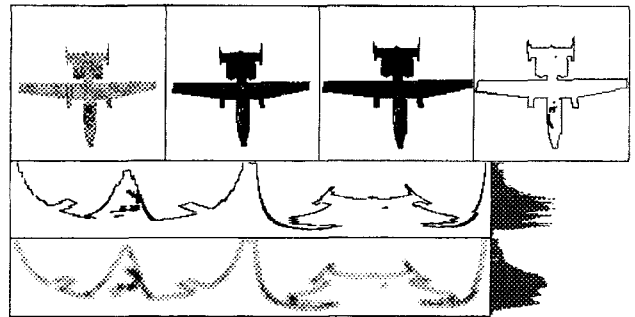


Fig. 1 Feature extraction example (A-10)

Table 1: Comparison of recognition rate of modular mART with single mART and SOM

Models of targets	Number of patterns	Recognition rate, %		
		Modular mART	Single mART	SOM
A-10	343	67.64	67.64	60.93
F-15	376	32.18	30.05	7.45
F-16	451	54.32	51.66	25.06
F-18	415	56.39	58.80	0.00
Mig-21	430	74.42	65.35	59.53
Mig-29	387	41.34	14.47	4.39
Mirage 2000	353	61.19	41.08	15.58
Su-27	464	63.15	47.20	32.97
Tornado	334	50.90	26.95	22.75
BMP-2	179	81.01	69.83	27.37
M-203	151	72.85	60.93	47.68
SAM Launcher	171	61.99	50.88	22.81
T-72	214	71.50	46.73	50.47
ZSU-23-4	208	92.79	88.94	83.17
Average	Ttl. 4476	62.98	51.47	32.87

Experimental results: Some experiments for three dimensional (3D) target recognition are carried out with 4,476 feature data gathered from nine planes and five tanks, as listed in Table 1. In this Letter, the unit circle normalisation method fixing the centre of gravity is used to obtain the shift and scaling invariance, and the polar transform is used to obtain the 2D rotation invariance. Fig. 1 shows an example of the feature extraction procedures applied to the A-10 fighter.

As shown in Fig. 1, the centre of gravity, which is used as the centroid, was located from the silhouette of the raw image. After the unit circle normalisation and the edge detection process, the polar coordinate transformation is carried out. The pattern in polar coordinates is manipulated by a lowpass filter to increase its adaptiveness. The circular projective histogram shown on the bottom right of the Figure is used as the input data of the mART neural networks.

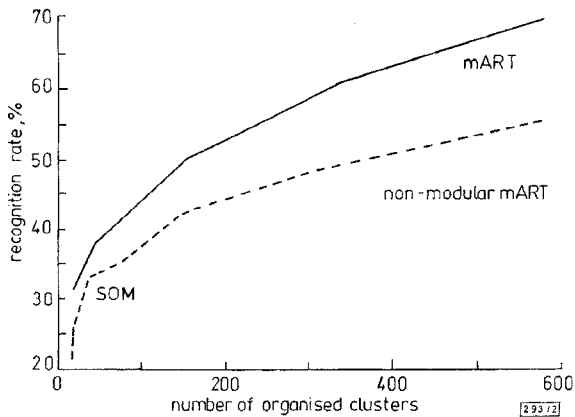


Fig. 2 Comparison of recognition rate of modular mART with single mART and SOM according to number of created clusters

As shown in Table 1, on average, the mART of a modular structure shows a rather good recognition rate of 62.98%, while that of the single mART is 51.47% and that of the general self-organising map (SOM) is 32.87%. The representative graph in Fig. 2 shows the recognition rates of mART, non modular mART and SOM against the number of clusters. The number of clusters is controlled by the threshold ρ of the similarity test. This graph shows that the modular mART, whatever the number of clusters, provides the highest recognition rate, compared with the general SOM and single mART.

Conclusions: In this Letter, we proposed the mART neural networks with a modular structure. We showed that since the organised clusters of the neural networks were trained by supervised modular learning and were optimised, they can rarely be misclassified into the other classes. From the 3D target recognition experiments, the system shows improvements of 22 and 92% in recognition rate compared with the single mART and the SOM, respectively.

© IEE 1997

12 May 1997

Electronics Letters Online No: 19970908

Eun-Soo Kim, Jin-Woo Cha and Chung-Sang Ryu (Department of Electronic Engineering, Kwangwoon University, #447-1, Wolge-Dong, Nowon-Ku, Seoul 139-701, Korea)

E-mail: eskim@daisy.kwangwoon.ac.kr

References

- BHANU, B.: 'Automatic target recognition: state of the art survey', *IEEE Trans. Aerosp. Electron. Syst.*, 1986, **AES-22**, (4), pp. 364-379
- WAIBEL, A., SAWAI, H., and SHIKANO, K.: 'Modularity and scaling in large phonemic neural networks', *IEEE Trans. Acoust. Speech Signal Process.*, 1989, **37**, (12), pp. 1888-1898
- KIM, E.-S., CHA, J.-W., and RYU, C.-S.: 'Three-dimensional target recognition using mART neural networks'. Proc. SPIE, April 1997, Vol. 3069

Composite optical/electrical buffer configuration for photonic ATM switching systems

T. Okugawa, T. Matsunaga and K. Habara

Indexing terms: Photonic switching systems, Asynchronous transfer mode, Buffer circuits

The proposed optical/electrical buffer configuration for optical-frequency routing in ATM switching systems provides low cell-loss probability and uses fewer optical devices since electrical buffers are used to share the buffering load. The shared-load balance is finely tuned by using an intermediate degree-of-multiplexing table.

Introduction: The optical-frequency-routing ATM switching system is a candidate for high-throughput switching nodes because of its high-speed and frequency multiplexing. For controlling contention, an output-type buffer configuration is preferable because of its low cell-loss probability characteristics. Either an all-optical or all-electrical buffer configuration can be used, but with an all-optical configuration, it is difficult to integrate a large number of optical components. With an all-electrical buffer configuration, many O/E converters and high bit rate large-scale electrical cell selectors are required because optical-frequency-multiplexed cells have to be demultiplexed and converted to electrical ones.

In this Letter, we propose a composite optical/electrical buffer configuration that overcomes these problems. In it, the buffering load is shared by optical and electrical buffers. We have evaluated its performance by calculation, using two optical-buffer-block configurations. The shared-load balance is tuned by using an intermediate degree-of-multiplexing table.

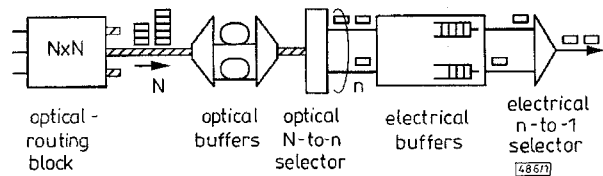


Fig. 1 Photonic ATM switching system including proposed optical/electrical buffer configuration

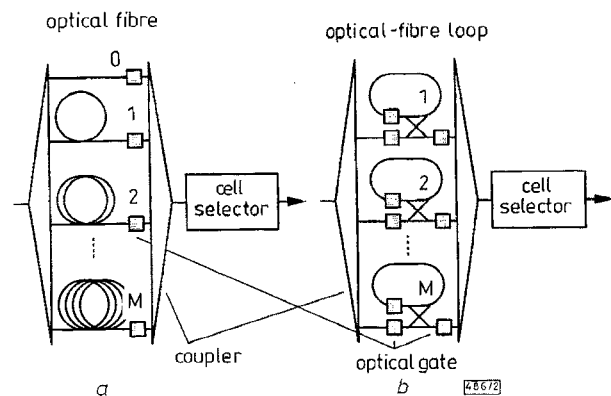


Fig. 2 Optical buffer block

a Travelling-type
b Circulating-type

Optical/electrical buffer configuration: A photonic ATM switching system including the proposed optical/electrical buffer configuration is shown in Fig. 1. An N -input N -output optical routing block routes cells to their destinations. This routing can be performed by using either a broadcast-and-select configuration [1] or frequency-routing using a tunable laser and a frequency router, such as by using an arrayed waveguide grating filter [2] configuration [3]. Although only one cell arrives at each input port at a time, several cells with different frequencies can be sent to an output port at the same time. Therefore, each output port must have a multi-input buffer memory. In the proposed buffer configuration, the optical buffer block holds cells that are frequency-